JOURNAL OF CHEMICAL & ENGINEERING DATA

ARTICLE

pubs.acs.org/jced

Validation and Prediction of the Temperature-Dependent Henry's Constant for CO_2−Ionic Liquid Systems Using the Conductor-like Screening Model for Realistic Solvation (COSMO-RS)

Yamini Sudha Sistla and Ashok Khanna*

Department of Chemical Engineering, Indian Institute of Technology Kanpur, Kanpur-208016, India

Supporting Information

ABSTRACT: Henry's constant H of carbon dioxide in a number of ionic liquids (ILs) has been studied using the predictive method COnductor-like Screening MOdel for Realistic Solvation (COSMO-RS). Experimental H values for 14 CO_2−IL systems spread over a temperature range of (283 to 333) K have been used to estimate the parameters λ_1 and λ_2 of the combinatorial term to calculate the chemical potential. The H values of CO_2 in 18 other ILs have been validated and found to be in good agreement with the experimental data with a relative deviation of less than 10 %. Cation groups like imidazolium, pyridinium, ammonium, uronium, thiouronium, and phosphonium have been studied. A total of 12 anions such as L^-, BF_4^-, $EtSO_4^-$, TFA^-, $OctSO_4^-$, Tf_2N^-, $mFAB^-$, $eFAB^-$, $mFAP^-$, $eFAP^-$, $pFAP^-$, and $bFAP^-$ were studied to find the most favorable cation and anion combination for high CO_2 solubility. It was observed that increasing the fluorination of organic anions containing fluoro alkyl groups gave lower Henry's constant values (following the trend $TFA^- > Tf_2N^- > mFAB^- > eFAB^- > mFAP^- > eFAP^- > pFAP^- > bFAP^-$), thus showing higher CO_2 solubility. Among the cations studied, phosphonium-based cations are found to be most promising for higher solubility. It was observed that the entropic effects (combinatorial) arising due to the size and shape of ILs play a major role in the estimation of H values, whereas the enthalpic effects (residual) arising due to molecular interactions have a minor but significant role. A correlation has been developed to predict the H of the $[R_n mim]^+$ cation-based IL by considering a reference value H_2 of $[R_2 mim]^+$. A common predictive equation has been developed to determine the temperature-dependent H values of CO_2 in any cation/anion combination of ILs.

1. INTRODUCTION

The increasing global emissions of greenhouse gases, especially carbon dioxide (CO_2), have been recognized as the main cause for global warming. The main sources of CO_2 generation are the coal-fired power plants, natural gas power generation plants, refineries, and gas processing units. Carbon capture and sequestration (CCS) has been identified as a key strategy to significantly reduce CO_2 emissions into the atmosphere. Currently, CO_2 capturing methods are being continuously developed based on experimental and modeling studies. These include: (a) amine scrubbing, (b) wet scrubbing with physical absorption, (c) chemical absorption, (d) adsorption on solid sorbents, and (e) membrane-based gas separation.[1] Conventional amine scrubbing is highly energy-intensive. Monoethanolamine (MEA), diethanolamine (DEA), and methyldiethanolamine (MDEA) are highly corrosive and volatile, causing fast solvent degradation and low thermal stability. A postcombustion CO_2 capture process involves cooling and subsequent reheating of the stream gas. This decreases the plant efficiency and thus increases the overall costs. As the desorption of CO_2 from amines is normally accomplished by heating the solvent to higher temperatures, the reusability of these amine solvents will be reduced because high volatilization of the amine solvent also takes place at such temperatures. At present, the regeneration of solvent is usually done by the pressure swing step. By using solvents which are stable up to higher temperatures [(422 to 644) K] the energy penalty connected with CO_2 compression could be reduced, and the regeneration can be done using a temperature swing.[2] The desirable properties of a potential solvent for CO_2 include: (a) a Lewis basicity to show strong affinity toward CO_2, which is a Lewis acid, (b) a high thermal stability to reduce solvent degradation at high temperatures, (c) being environmentally friendly, (d) a negligible vapor pressure, (e) being less corrosive, (f) the ability to absorb CO_2 without much cooling of humid gas streams, (g) a high regeneration efficiency, and (h) a low enough viscosity.[3−5]

In the exploration of new solvents to replace the conventional amine solvents, extensive research efforts by several groups[6−9] suggested that ionic liquids (ILs), which are liquids at room temperature (<100 °C), can be a promising alternative. ILs have negligible (or zero) vapor pressure (nonvolatile) and are thermally stable (start decomposing above 300 °C) and thus have less solvent degradation.[6] The ILs contain an organic cation and an inorganic/organic anion. The cations of ILs consist of imidazolium, pyridinium, pyrolidium, phosphonium, guanidinium, uronium, and so forth. The anions of ILs include tetrafluoroborate (BF_4), dicyanamide (DCA), hexafluorophosphate (PF_6), nitrate (NO_3), trifluoromethanesulfonate (TfO), trifluoroacetate (TFA), bis[(trifluoromethyl)sulfonyl]imide (Tf_2N), and tris(trifluoromethyl)trifluorophosphate (mFAP).[7] The physical properties like melting point, density, and viscosity

Received: May 19, 2011
Accepted: September 26, 2011
Published: October 13, 2011

ACS Publications © 2011 American Chemical Society

of the ILs can be tuned by changing the substituents of the cation or anion and thus giving the name "designer solvents" to ILs. Compounds with dipole moments (e.g., water) and those which show specific interactions like hydrogen bonding and compounds having quadrupole moments (e.g., CO_2, N_2O) are found to be highly soluble in ILs.[8,9]

For the CO_2 capture application, both the cation and the anion of the IL have an influence on the CO_2 absorption ability in the IL.[6] However, the anion−CO_2 interaction is a dominant mechanism compared to that of the cation−CO_2 interaction in the CO_2 absorption process.[8] In the context of the cation, the acidic protons of the cation (e.g., hydrogen atom of C_2 carbon on the imidazolium cation-based IL) are likely the sites that are favorable for the interaction between the O atom of CO_2 and hydrogens of the cation.[36] Besides, for the imidazolium-based ILs, the length of alkyl chain attached to imidazolium cation ring was also found to affect the CO_2 absorption.[4] The general trend was that, as the length of the alkyl chain increases, the CO_2 solubility increases. This was attributed to favorable CO_2 absorption into the free spaces (interstices) formed in the IL network due to the steric hindrances resulted by the long alkyl chains.[10,11] However, the anion of the IL has much stronger interaction with CO_2 relative to the cation of the IL.[5,6,9] This is believed to be mainly due to Lewis acid−base interactions between the electron-poor carbon atom and electronegative atoms (e.g., fluorine) associated with the anion of the IL.[6,9,10] It is clear from the reported studies above that the anion of the IL plays a key role in CO_2 absorption ability, while the cation plays a secondary role or it has a less effect on CO_2 solubility, in other words. In particular, anions containing fluoroalkyl groups were found to show high CO_2 solubility, which increases in the order: eFAP > Tf_2N > TfO > PF_6 > DCA > BF_4 > NO_3. To date, many of the researchers have studied the CO_2 solubility in various ILs. The CO_2 solubility in ILs is of the order of almost 0.50 mole fraction at pressures around 50 bar.[6]

In search for potential ILs for carbon dioxide capture applications, computational methods play an important role. Computational methods not only reduce the cost of experimentation but also assist in designing new "task-specific" ILs.[7] Knowledge of CO_2 solubility in ILs is very important to find the most suitable ILs for the effective CO_2 capture. The solubility of a gas in a liquid is often described in terms of Henry's law constant. The lower the Henry's constant, the higher the solubility.[14] This work aims at accurately predicting Henry's constant of CO_2 in ILs using the COnductor like Screening MOdel for Realistic Solvation (COSMO-RS).[12] The selection of COSMO-RS for the present study was made based on the following reasons. In general, the activity coefficient models, such as nonrandom two-liquid (NRTL), Wilson, and universal quasichemical activity coefficient (UNIQUAC) models, and so forth, deal with fitting the experimental data to a given functional form. The thermodynamic information subsequently is extracted from that functional form. In addition, there are also other methods like group contribution methods (GCM) like the universal functional acitivity coefficient model (UNIFAC), and so forth. These methods do not depend on experimental thermodynamic data. In these methods, estimates are obtained from molecular structure information only. GCMs are based on interaction parameters that have been obtained previously by analysis of the phase equilibrium data of systems containing the same functional groups. [24] All of these models can be used for the property predictions, provided sufficient experimental data is available. But, all of these methods do not consider the molecular details of the compounds of interest. Therefore, the above-mentioned methods can fail in case of new types of compounds. A more fundamental description of molecular interactions can be predicted using quantum chemical calculations using molecular simulations. [18,22] Thus, the present study chooses the COSMO-RS method, which considers both quantum chemical calculations of individual molecules and statistical thermodynamics to predict the various thermodynamic properties of the mixtures.

Zhang et al.[13] have already reported the Henry's constant of CO_2 in a number of ILs only at 298 K using COSMOThermX software;[15] however, there are some significant deviations between their computational and their experimental values. Recently Palomar et al.[14] also have reported the H values of CO_2 in 156 ILs using COSMOThermX software. The present study considers several ILs containing a wide variety of anions and cations. In the present study, COSMO files generated using Gaussian 03[30] are used as input to our own developed MATLAB code based on COSMO-RS theory.[12] Initially, the H values are predicted and successfully validated for 18 CO_2−IL systems at different temperatures ranging from (283 to 333) K. The predicted Henry's constants are in close correspondence with the experimental H values reported.[6,13,38−45] After validation, the H values of CO_2 in 228 ILs are predicted at four different temperatures [(283, 298, 323, and 333) K]. Additionally, the predictive equations are developed for the estimation of H values with respect to alkyl chain length for the imidazolium cation-based ILs. A generalized universal equation is also developed for the temperature dependence of Henry's constant. The effect of amine functionalization of imidazolium cation-based ILs on CO_2 solubility is also considered since amine tethering to imidazolium cation of IL resulted in an increase of CO_2 solubility.[7]

2. COSMO-RS THEORY AND BACKGROUND

Klamt[12] and co-workers developed a novel method called COSMO-RS in 1994, to predict thermophysical properties of pure and mixed compounds. The COSMO-RS method is the combination of the COSMO model with statistical thermodynamics. In the COSMO-RS approach the ensemble of interacting molecules is replaced by the corresponding ensemble of independent, pairwise interacting surface pieces.[16] For fluid phase simulations, almost all of the computational chemistry methods start with vacuum (dielectric constant $\varepsilon = 1$) as a reference state. The COSMO-RS theory has introduced a state of molecules in a conductor ($\varepsilon = \infty$) as a conceptually fruitful method for the fluid phase simulations.[24] Initially, for the COSMO-RS approach, COSMO files using quantum chemical (QC) methods are generated through an algorithm which is divided into 8 steps: (1) An initial geometry of the solute molecule is obtained from Gaussian 03.[30] (2) A cavity (usually defined by the exterior of the atom-centered spheres) defining the boundary of the conductor is constructed around the solute, which is subsequently divided into small surface segments. (3) The quantum chemical method generates an initial electron density of the solute. (4) The solute electrostatic potential arising from the atomic nuclei and electron density is calculated on the grid of cavity segments. (5) The conductor screening charge density σ is calculated from the conductor boundary conditions such that the electrostatic

Table 1. Parameters Used for the COSMO-RS Calculations[24]

parameter	value
a_{eff}	6.25 Å^2
α'	5950 (kcal·Å^4)·(mol·e^2)$^{-1}$
c_{hb}	54873 (kcal·Å^4)·(mol·e^2)$^{-1}$
σ_{hb}	0.0085 e·Å^{-2}

potential arising from the solute and the corresponding polarization charges on the cavity vanishes on the entire surface. (6) The polarization charges are included as external charges in the quantum chemical iteration resulting in a modified electron density. (7) A correction for outlying charge errors arising from the small portion of electron density outside the cavity is applied iteratively to the total energy and to the polarization charge densities. (8) The gradient of the total QC/COSMO energy is calculated analytically from the converged electron density and polarization charges and is used to reach a optimal geometry at lower energy.[24]

The above eight steps of COSMO algorithm give the (a) energy, (b) electron density, (c) polarization charge densities, (d) geometry of the molecule in the virtual conductor[18−24] (e) molecular surface area, and (f) molecular volume. Gaussian 03[30] gives this data as the .cosmo files.

To calculate the thermodynamic averages of all possible liquid configurations, the concept of σ profiles has been introduced. A σ profile is a histogram of the molecular COSMO surface, with respect to polarization charge density. The ensemble of surface pieces characterizing a liquid system S is described by the probability distribution function $p_S(\sigma)$ which gives the probability of surface in the ensemble having a screening charge density between σ and $\sigma + d\sigma$; termed as the σ-profile. For a mixture consisting of several compounds X_i with molar concentrations x^i, the σ-profile of the system is given by the weighted sum of the σ-profiles of all of the components.[20−24]

$$p_S(\sigma) = \sum_{i \in S} x^i p^{X_i}(\sigma) \quad (1)$$

where $p^{X_i}(\sigma)$ is the relative amount of surface with polarity σ on the surface of molecule.

The COSMO-RS calculations use four basic parameters: (1) effective contact area a_{eff}, which determines the number of independent neighbors of a molecule, (2) electrostatic misfit energy coefficient α' and self-energy of a single segment of surface a_{eff} divided by surface charge density σ, (3) threshold constant for hydrogen bonding σ_{hb}, and (4) strength coefficient c_{hb}. For the present study, the values of all of the above parameters are taken from Klamt et al.[25] as shown in Table 1. Preliminary screening of the three options (Klamt et al.[25] vs Banerjee et al.[28]) available revealed a better match with the experimental values with the Klamt's parameters which are shown in Table 1.

From the σ-profiles of a liquid system, the σ-potential can be calculated by integration over all potential partners σ' in the liquid S.

$$\mu_S(\sigma) = -\frac{RT}{a_{eff}} \ln\left[\int p_S(\sigma') \exp\left(\frac{a_{eff}}{RT}(\mu_S(\sigma') - E_{misfit}(\sigma,\sigma') - E_{hb}(\sigma,\sigma'))\right) d\sigma'\right] \quad (2)$$

where the σ-potential $\mu_S(\sigma)$ is the specific chemical potential which is a measure of the affinity of a system S to surface of polarity σ. The above eq 2 states that the chemical potential per surface area of a piece of surface polarity σ in the solvent ensemble characterized by the solvent σ-profile.

The electrostatic misfit energy E_{misfit} is described in terms of the polarization charges of the two interacting species σ and σ' as,

$$E_{misfit}(\sigma,\sigma') = a_{eff}\frac{\alpha'}{2}(\sigma + \sigma')^2 \quad (3)$$

The energy due to hydrogen-bonding energy E_{hb} is described in terms of the polarization charges of the hydrogen bond donor σ_{donor} and acceptor $\sigma_{acceptor}$ as:

$$E_{hb} = a_{eff} c_{hb} \min(0; \min(0; \sigma_{donor} + \sigma_{hb}) \max(0; \sigma_{acceptor} - \sigma_{hb})) \quad (4)$$

where $\sigma_{don} = \min(\sigma,\sigma')$ and $\sigma_{acc} = \max(\sigma,\sigma')$.

In addition to the interaction energies which depend on the screening charge density σ, there is a van der Waals interaction energy E_{vdW} which is dependent on the type of the atomic elements and is expressed as:

$$E_{vdW} = a_{eff}(\tau_{vdW} + \tau'_{vdW}) \quad (5)$$

where a_{eff} is the effective contact area between the two atoms. τ_{vdW} and τ_{vdW}' are the atom specific van der Waals constants. It can be observed from above that eqs 3 and 4 are functions of screening charge density σ and eq 5 depends on the effective contact area and the van der Waals constants of the specific elements. Thus, the screening charge density σ is an important descriptor in determining the interaction energies.

Equation 2 above is solved iteratively for the chemical potential. To simplify the above equation, an expression for activity coefficient $\gamma_S(\sigma)$ is defined as

$$\ln \gamma_S(\sigma) = \mu_S(\sigma)/RT \quad (6)$$

Rewriting the equation for chemical potential

$$\ln \gamma_S(\sigma) = -\ln\left\{\int d\sigma' p'_S(\sigma')\gamma_S(\sigma')\exp\left(-\frac{a_{eff}e(\sigma,\sigma')}{RT}\right)\right\} \quad (7)$$

where $p'_S(\sigma')$ is the normalized σ-profile of the system which is defined as

$$p'_S(\sigma') = p_S(\sigma)/A_S = p_S(\sigma)/\sum_{i \in S} x^i A^{X_i} \quad (8)$$

where A^{X_i} is the molecular area of each component of the system

The chemical potential of solute X_i in a solvent S can now be calculated by integration of $\mu_S(\sigma)$ over the surface of the solute compound. The chemical potential can be written as the sum of residual and combinatorial terms:

$$\mu_S^{X_i} = \int p^{X_i}(\sigma)\mu_S(\sigma)\, d\sigma + \mu_{C,S}^{X_i} \quad (9)$$

where $\int p^{X_i}(\sigma)\mu_S(\sigma)\, d\sigma$ is the residual term that accounts for the enthalpy effect of the system and $\mu^{X_i}_{C,S}$ is the combinatorial term that accounts for the entropy (size and shape) effect of the system.

dx.doi.org/10.1021/je200486c |J. Chem. Eng. Data 2011, 56, 4045–4060

Table 2. Names, Abbreviations, and Structures of Different Cations and Anions of ILs

Name of the ion	Abbreviation	Structure
Cation		
1-**e**thyl-3-**m**ethyl**im**idazolium; $R_1=C_2H_5$, $R_2=CH_3$ 1-**p**ropyl-3-**m**ethyl**im**idazolium; $R_1=C_3H_7$, $R_2=CH_3$ 1-**b**utyl-3-**m**ethyl**im**idazolium; $R_1=C_4H_9$, $R_2=CH_3$ 1-**pe**ntyl-3-**m**ethyl**im**idazolium; $R_1=C_5H_{11}$, $R_2=CH_3$ 1-**h**exyl-3-**m**ethyl**im**idazolium; $R_1=C_6H_{13}$, $R_2=CH_3$ 1-**o**ctyl-3-**m**ethyl**im**idazolium; $R_1=C_8H_{17}$, $R_2=CH_3$ 1-**a**mino**p**ropyl-3-**m**ethyl**im**idazolium; $R_1=C_8II_{17}$, $R_2=CII_3$ 1-**p**ropyl-3-**b**utyl**im**idazolium; $R_1=C_3H_7$, $R_2=C_4H_9$ 1-**a**mino**p**ropyl-3-**b**utyl**im**idazolium; $R_1=C_3H_8N$, $R_2=C_4H_9$ 1-**dim**ethyl**a**mino**p**ropyl-3-**b**utyl**im**idazolium; $R_1=C_5H_{12}N$, $R_2=C_4H_9$ 1-**v**inyl**b**enzyl-3-**b**utyl**im**idazolium; $R_1=C_3H_7$, $R_2=C_4H_9$	$[emim]^+$ $[pmim]^+$ $[bmim]^+$ $[pemim]^+$ $[hmim]^+$ $[omim]^+$ $[apmim]^+$ $[pbim]^+$ $[apbim]^+$ $[dmapbim]^+$ $[vbbim]^+$	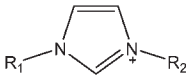
1-N-**b**utyl-3-**m**ethyl**py**ridinium; $R=C_4H_9$ 1-N-**h**exyl-3-**m**ethyl**py**ridinium; $R=C_6H_{13}$	$[bmpy]^+$ $[hmpy]^+$	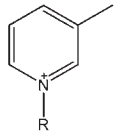
O-**e**thyl-*N,N,N′,N′*-tetramethyliso**u**ronium; $R=C_2H_5$	$[ETU]^+$	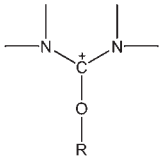
S-**E**thyl-*N,N,N′,N′*-**t**etramethyliso**th**io**u**ronium; $R=C_2H_5$ S-**P**ropyl-*N,N,N′,N′*-tetramethyliso**th**io**u**ronium; $R=C_3H_7$	$[ETTU]^+$ $[PTTU]^+$	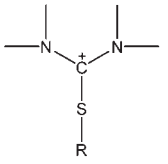
(p-**v**inyl**b**enzyl)**tri**methyl**a**mmonium	$[VBTMA]^+$	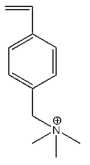
[2-(**m**eth**a**cryloyloxy)ethyl]**tri**methyl**a**mmonium	$[MATMA]^+$	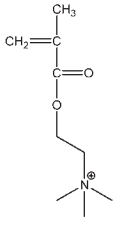
Trihexyltetra**d**ecyl**p**hosphonium	$[P_{(14)666}]^+$	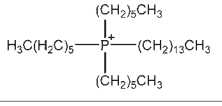
Anion		
Lactate	$[L]^-$	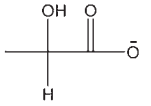

dx.doi.org/10.1021/je200486c |*J. Chem. Eng. Data* 2011, 56, 4045–4060

Table 2. Continued

Name of the ion	Abbreviation	Structure
Ethyl **s**ulfate; R = C_2H_5 **Oct**yl **s**ulfate; R = C_8H_{17}	$[EtSO_4]^-$ $[OctSO_4]^-$	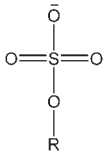
Trifluoro**a**cetate	$[TFA]^-$	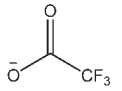
Tetrafluoro**b**orate	$[BF_4]^-$	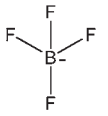
Trifluoro**m**ethyltrifluoro**b**orate	$[mFAB]^-$	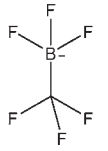
Bis(**tri**fluoromethyl**s**ulfonyl)**i**mide	$[Tf_2N]^-$	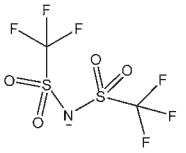
Penta**f**luoro**e**thyltrifluoro**b**orate	$[eFAB]^-$	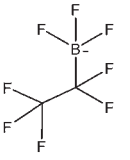
Tris(trifluoro**m**ethyl)trifluoro**p**hosphate	$[mFAP]^-$	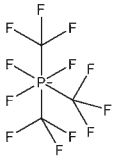
Tris(pentafluoro**e**thyl)trifluoro**p**hosphate; R=C_2F_5 Tris(heptafluoro**p**ropyl)trifluoro**p**hosphate; R=C_3F_7 Tris(nonafluoro**b**utyl)trifluoro**p**hosphate; R=C_4F_9	$[eFAP]^-$ $[pFAP]^-$ $[bFAP]^-$	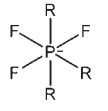

$p^{X_i}(\sigma)$ is the σ-profile of the solute, and $\mu_S(\sigma)$ is the chemical potential of the solution.

The combinatorial term depends on the area and volume of all of the compounds in the mixture and three adjustable parameters $(\lambda_0, \lambda_1, \lambda_2)$.[26]

$$\mu_{C,S}^{X_i} = RT\left[\lambda_0 \ln r_i + \lambda_1\left(1 - \frac{r_i}{r} - \ln \bar{r}\right) + \lambda_2\left(1 - \frac{q_i}{q} - \ln \bar{q}\right)\right] \quad (10)$$

where r_i is the molecular volume and q_i is the molecular area of compound *i*. The output file with the .cosmo extension generated during COSMO calculations in GAUSSIAN gives the molecular surface area q_i and volume r_i for the COSMO cavity of the molecule. The total volume and area for the mixture being

$$\bar{r} = \sum_i x_i r_i \qquad \bar{q} = \sum_i x_i q_i \quad (11)$$

λ_0, λ_1, and λ_2 are three adjustable parameters.

The combinatorial term for the pure compound is given as

$$\mu_{C,X}^{X} = -\lambda RT \ln q \quad (12)$$

The chemical potential thus obtained is used to estimate thermodynamic properties of pure compounds and mixtures. The detailed

dx.doi.org/10.1021/je200486c |*J. Chem. Eng. Data* 2011, 56, 4045–4060

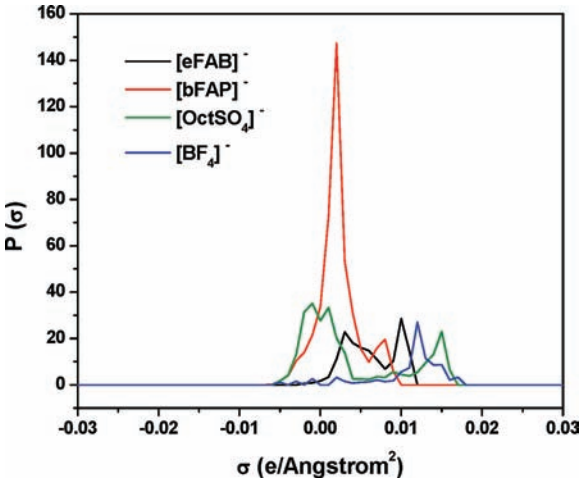

Figure 1. σ-profiles of some anions.

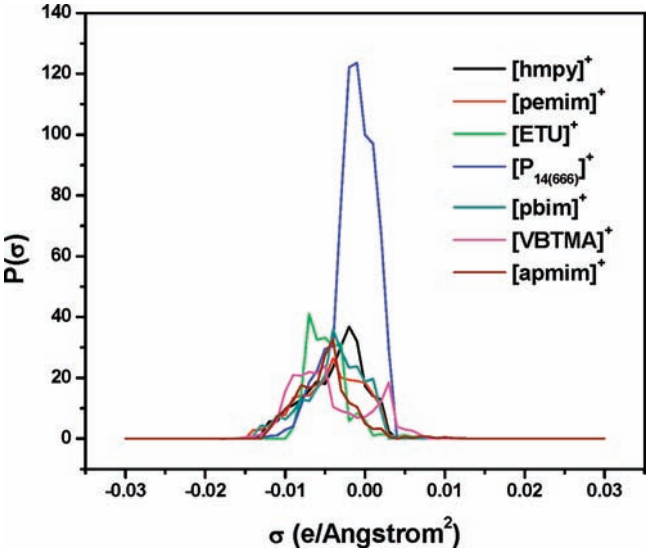

Figure 2. σ-profiles of various cations.

theory of COSMO-RS can be found in Klamt's papers,[12,17−21,23−25,27] Freiria et al.,[22] and the COSMOThermX user manual.[26]

Henry's Constant. Henry's law states that the solubility of a gas in a liquid solution at a constant temperature is proportional to the partial pressure of the gas above the solution.

The infinite dilution activity coefficient γ^{∞} of solute X in a solvent S is calculated through[27−29]

$$\gamma^{\infty} = \lim_{x \to 0} \gamma_S^X = \lim_{x \to 0} \exp\left(\frac{\mu_S^X - \mu_X^X}{RT}\right) \quad (13)$$

where γ_S^X is the activity coefficient of the solute X_i in solvent S, μ_S^X is the chemical potential of the solute X_i in solvent S, and μ_X^X is the pure component chemical potential of the solute so that the Henry's constant is

$$H = \lim_{x \to 0} \gamma_S^X p^0 = \gamma_S^{X\infty} p^0 \quad (14)$$

where $\gamma_S^{X\infty}$ is the infinite dilution activity coefficient of solute in the solvent and p^0 is the pure component vapor pressure of

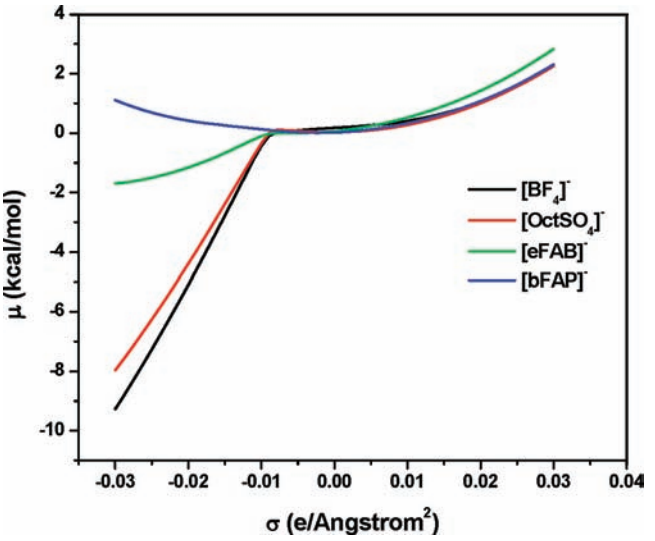

Figure 3. σ-potentials of some anions.

the solute gas. Here, the vapor pressure p^0 for CO_2 is determined by using the DIPPR equation provided by Carvalho and Coutinho.[38]

$$p^0_{CO_2} = \exp[140.54 - 4735/(T/\mathrm{K}) - 21.68\ln(T/\mathrm{K}) + 0.040909(T/\mathrm{K})] \quad (15)$$

The critical point of CO_2 is at 304 K and 74.7 atm. The conditions used [(283 to 333) K, 1 atm] in the present study do not correspond to the critical conditions of CO_2. The eq 15 has been used for calculating the vapor pressure of CO_2 at all temperatures [(283, 298, 323, and 333) K] considered here. Carvalho and Coutinho[38] applied eq 15 at a wide range of conditions and even for conditions above the critical point of CO_2. They have obtained $P-x$ predictions that match well with the experimental data of the CO_2−IL systems at all of the conditions applied.

To date, many researchers[13−16] have used the COSMO-RS method to estimate Henry's constants for gas solubility in conventional solvents. The objective of the present work is to validate the Henry's constant of CO_2 obtained from the COSMO-RS method with the experimental values available and to predict the H values for a number of ILs at different temperatures [(283, 298, 323, and 333) K].

3. COMPUTATIONAL DETAILS

The IL is considered as an equimolar mixture of cation and anion.[28,29] The cations are selected such that they cover a wide variety of cationic groups like imidazolium, pyridinium, ammonium, uronium, thiouronium, and phosphonium. Among the anions available, some of the fluorinated and some of the nonfluorinated anions were selected. The geometry optimization of all of the isolated cations and anions are done using a quantum chemistry package Gaussian 03[30] with the density functional theory (DFT) method B3LYP[32,33] and 6-31G**[34] basis set. The frequency analysis has also been carried out at the same basis set to check the absence of negative frequencies which makes sure that the molecule has attained a true minimum. The input for Gaussian 03 was made in the visualization software MOLDEN.[31] The names, abbreviations, and the structures of the cations and anions of the ILs considered in the present study are given in

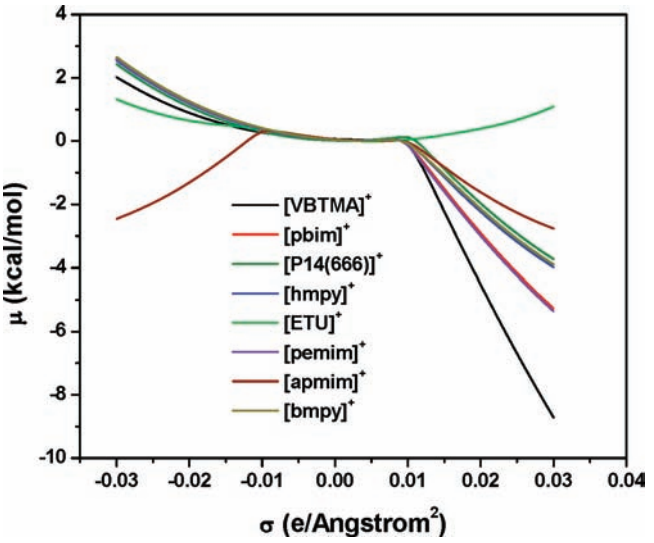

Figure 4. σ-potentials of various cations.

Table 2. After attaining the equilibrium geometry with the minimum energy structure for each cation and anion, COSMO files are then generated using DFT BP86[32,35] with a triple-ζ valence polarization (TZVP)[36] basis set in combination with density fitting basis set DGA1[37] using Gaussian 03. The resultant COSMO output file contains the energy, electron density, polarization charge densities, and the geometry of the molecule in a virtual conductor. The σ-profiles and σ-potentials were then generated for all cations and anions from the polarization charge densities. The σ-profiles of some anions and cations are shown in Figures 1 and 2, respectively. Also, the σ-potentials of few anions and cations are shown in Figures 3 and 4, respectively. These σ-profiles and σ-potentials are useful in calculating the residual contribution of the chemical potential of the solute CO_2 in the solvent IL (which is the enthalpy contribution arising due to the strength of chemical bonds in the molecular structures).

For the basis set selection in the above computations, as the nature of the electron clouds of the anions is more diffuse than that of the neutral species or cations, the aug-cc-pVTZ (augmented-correlation consistent-polarized valence triple-ζ) basis set was also attempted. However, a comparison between the predictions of H values of CO_2 in some ILs for aug-cc-pVTZ and TZVP basis sets showed that the predictions obtained by the TZVP basis set match well with the experimental values compared to those obtained by the aug-cc-pVTZ basis set. Thus, the TZVP basis set was ultimately selected as the basis set for the present study. The comparison between two basis sets is provided in the Supporting Information.

4. PREDICTION OF PARAMETERS

While calculating the chemical potential of pure compounds, the value of the parameter λ of the combinatorial term is taken as 0.14.[20−24] The combinatorial term of the system for a mixture of compounds has three adjustable parameters: λ_0, λ_1, and λ_2. From eq 10 we can observe that λ_0 is a parameter corresponding to the solute only. Therefore by fixing $\lambda_0 = 0.14$,[20−24] the other two parameters λ_1 and λ_2 were calculated by optimizing a set of experimental data. Out of available 32 experimental literature H values of CO_2 in various ILs at different temperatures, initially we considered 10 experimental H values corresponding to 298 K to obtain the λ values ($\lambda_1 = -0.0116$, $\lambda_2 = 0.3971$). But these

Table 3. Henry's Constant of CO_2−IL Systems Used for the λ_1 and λ_2 Estimation

sample no.	IL	temperature (K)	experimental literature H value (MPa)	reference
1	$[emim]^+[TFA]^-$	298	4.3	40[a,b]
2	$[emim]^+[Tf_2N]^-$	298	3.13	40[a]
3	$[pmim]^+[Tf_2N]^-$	298	3	42[b]
4	$[bmim]^+[BF_4]^-$	323	8.86	6[b]
5	$[bmim]^+[BF_4]^-$	298	5.6	40, 41[a]
6	$[bmim]^+[Tf_2N]^-$	298	3.43	10[a]
7	$[bmim]^+[Tf_2N]^-$	283	2.53	43[b]
8	$[pemim]^+[bFAP]^-$	333	3.29	9[b]
9	$[pemim]^+[bFAP]^-$	298	2	9[b]
10	$[hmim]^+[BF_4]^-$	298	4.3	40[a]
11	$[hmim]^+[Tf_2N]^-$	323	4.56	9[b]
12	$[hmim]^+[Tf_2N]^-$	298	3	41[a]
13	$[hmim]^+[eFAP]^-$	333	4.2	9[b]
14	$[hmim]^+[eFAP]^-$	298	2.5	9[a]
15	$[hmim]^+[pFAP]^-$	298	2.16	9[b]
16	$[omim]^+[BF_4]^-$	298	4.3	40[b]
17	$[bmpy]^+[BF_4]^-$	298	5.4	39[a,b]
18	$[bmpy]^+[eFAP]^-$	298	2.85	13[a]
19	$[hmpy]^+[Tf_2N]^-$	298	3.28	5[b]
20	$[hmpy]^+[Tf_2N]^-$	283	2.54	9[b]
21	$[ETTU]^+[eFAP]^-$	298	2.94	13[a,b]

[a] The 10 systems used for the isothermal approach where all data is at 298 K. [b] The 14 systems used for the nonisothermal approach.

λ values were not able to accurately predict the H at other temperatures. Later, a set of new λ values were obtained by using the experimental literature data of 14 CO_2−IL systems at various temperatures ranging from (283 to 333) K. A complete list of the experimental data used for the two approaches is given in Table 3. The values of λ_1 and λ_2 obtained are 1.5630 and −1.3011, respectively. The optimization procedure for the calculation of parameters λ_1 and λ_2 is given in the Supporting Information. The H values thus obtained using the new set of λ values are compared with the existing 18 experimental literature data other than the 14 systems previously used for the prediction of λ values. The comparison of the validation of predicted H values using the two sets of λ values with the literature data are shown in Table 4. The root-mean-square deviation (rmsd), defined as rmsd = $(\sum_{i=1}^{N}(H_{pre,i} - H_{expt,i})^2/N)^{1/2}$, with the new λ values is found to be significantly reduced. The mean unsigned percent error is defined as MUPE = $[(1/N)\Sigma ABS((H_{pre} - H_{exp})/H_{exp})] \cdot 100$. The H values predicted by our method are compared with the Zhang et al.[13] and Palomar et al.[14] values and are presented in Table 5. The MUPE of our data at 298 K is 7 %, whereas that of Zhang et al. is 17 %. Also, Palomar et al. reported an MUPE of 20 %. This difference in MUPE could be due to the parametrization. The two parameters λ_1 and λ_2 in the COSMOThermX software could have been obtained by fitting to a large set of experimental data including nonionic liquids and gaseous compounds. We have optimized the two parameters λ_1 and λ_2 especially to make it applicable to CO_2−IL systems. Also there might be some difference in generating the .cosmo files which are the input files for the COSMO-RS program.

Table 4. Validation of Henry's Constant (H) Predictions against Experimental Literature Values

sample no.	IL	temperature	experimental literature H (MPa) value	predicted H, MPa (first approach)[a]	predicted H MPa (second approach)[b]	% deviation from expt H (second approach)	reference
1	$[emim]^+[Tf_2N]^-$	323	5.15	6.02	5.68	10.3	6
2	$[emim]^+[Tf_2N]^-$	298	3.13	3.3	3.27	4.4	6
3	$[emim]^+[Tf_2N]^-$	283	2.53	2.43	2.28	−9.8	6
4	$[bmim]^+[BF_4]^-$	298	5.6	5.3	5.57	−0.53	6, 44
5	$[bmim]^+[BF_4]^-$	283	4.08	3.69	3.87	−5.1	6, 44
6	$[bmim]^+[Tf_2N]^-$	323	4.87	5.62	5.38	10.4	44
7	$[bmim]^+[Tf_2N]^-$	298	3.43	3.12	3.09	−9.9	43
8	$[hmim]^+[BF_4]^-$	298	5.3	4.99	5.13	−3.2	40
9	$[hmim]^+[BF_4]^-$	283	3.8	3.58	3.58	−5.7	40
10	$[hmim]^+[Tf_2N]^-$	298	2.82	3	2.94	4.25	45
11	$[hmim]^+[Tf_2N]^-$	283	2.42	2.42	2.04	−15.7	45
12	$[hmim]^+[eFAP]^-$	298	2.37	2.6	2.27	−4.21	45
13	$[hmim]^+[pFAP]^-$	333	3.6	5.52	4.42	22.7	45
14	$[omim]^+[BF_4]^-$	283	3.2	3.48	3.36	5	39
15	$[omim]^+[Tf_2N]^-$	298	3	2.9	2.82	−6	43
16	$[bmpy]^+[Tf_2N]^-$	298	3.2	3.06	2.98	−6.8	40
17	$[bmpy]^+[eFAP]^-$	298	2.85	2.7	2.34	−17.8	13
18	$[hmpy]^+[Tf_2N]^-$	323	4.62	5.21	5.05	9.3	45
	rmsd					0.35	
	MUPE					8.40 %	

[a] Based on isothermal data at 298 K of Table 2. [b] Based on nonisothermal data of Table 2.

Table 5. Comparison of Henry's Constants at 298 K[a]

IL	literature (exptl)	present work	% deviation	Zhang et al.[13]	% deviation	Palomer et al.[14]	% deviation
$[bmpy]^+[BF_4]^-$	5.4	5.02	−7.04	4.2	−22.22		
$[hmim]^+[BF_4]^-$	5.3	5.13	−3.21	4.8	−9.43		
$[hmim]^+[Tf_2N]^-$	2.82	2.94	4.26	3.4	20.57	3.3	17.02
$[emim]+[Tf_2N]^-$	3.13	3.27	4.47	4.2	34.19	4.2	34.19
$[bmim]^+[Tf_2N]^-$	3.43	3.09	−9.91	3.7	7.87	3.6	4.96
$[bmpy]^+[Tf_2N]^-$	3.2	2.98	−6.88	3.3	3.12		
$[bmim]^+[BF_4]^-$	5.6	5.57	−0.54	5.4	−3.57	6.1	8.93
$[bmpy]^+[eFAP]^-$	2.85	2.34	−17.89	2	−29.82		
$[hmpy]^+[Tf_2N]^-$	3.28	2.88	−12.20	3.1	−5.49		
$[ETTU]^+[eFAP]^-$	2.94	2.58	−12.24	1.7	−42.18	1	−65.99
$[hmim]^+[pFAP]^-$	2.16	2.08	−3.70	2	−7.41		
$[hmim]^+[eFAP]^-$	2.37	2.27	−4.22	2	−15.61	1.9	−19.83
rmsd			0.28		0.69		0.96
MUPE			7.2		16.7		20

[a] References for experimental data are shown in Table 3.

5. RESULTS AND DISCUSSION

By substituting the values of the three parameters ($\lambda_0 = 0.14$, $\lambda_1 = 1.5630$, and $\lambda_2 = -1.3011$) in eq 10, Henry's constant (H) of CO_2 in a number of ILs comprising of different anions and cations at temperatures of (283, 298, 323, and 333) K and at atmospheric pressure is estimated using the COSMO-RS theory. These H values are validated for the 18 ILs (other than the 14 systems used for the parametrization) as shown in Table 4 and are found to be in good agreement with the experimental values with an MUPE of 8.4 %. The signed percent deviations in H values for each IL are also shown in Table 4. ILs such as [hmim][pFAP] and [bmpy][eFAP] have shown some deviation but still reasonably acceptable predictions. This discrepancy for these two ILs most likely due to the parametrization set since these ILs were not included in the parametrization set. We have deliberately not included some ILs for the parametrization purpose to validate the predictions with the experimental values. As can be seen from Tables 4 and 5, most of the predictions match well with the experimental values. Afterward, H values of CO_2 in a number of ILs at different temperatures are predicted. The relationship between the Henry's constant and the solubility of CO_2 can be understood by the definition of Henry's constant, which is expressed as

$$H = \lim_{x \to 0} \frac{p}{x} \tag{16}$$

dx.doi.org/10.1021/je200486c |J. Chem. Eng. Data 2011, 56, 4045–4060

Table 6. COSMO Volume, Surface Area, and Molecular Weight of Cations and Anions

cation	volume	area	mol wt	anion	volume	area	mol wt
$[emim]^+$	1015.61	605.37	111	$[BF_4]^-$	487.55	329.71	87
$[pmim]^+$	1153.33	681.02	123	$[TFA]^-$	631.11	410.57	113
$[bmim]^+$	1291.58	757.91	135	$[L]^-$	674.63	428.78	89
$[ETU]^+$	1329.08	767.61	145	$[mFAB]^-$	731.6	458.08	137
$[ETTU]^+$	1432.4	802.8	161	$[EtSO_4]^-$	807.75	498.87	125
$[bmpy]^+$	1407.4	806.42	150	$[eFAB]^-$	953.25	573.62	187
$[VBTMA]^+$	1491.29	816.12	176	$[mFAP]^-$	1345.44	719.62	295
$[pemim]^+$	1426.39	828.32	147	$[Tf_2N]^-$	1367.68	795.21	280
$[PTTU]^+$	1574.45	877.32	175	$[OctSO_4]^-$	1629.08	950.86	209
$[MATMA]^+$	1535.67	879.42	172	$[eFAP]^-$	2004.36	985.29	445
$[hmim]^+$	1564.42	904.69	159	$[pFAP]^-$	2705.2	1316.61	595
$[pbim]^+$	1566.36	908.3	167	$[bFAP]^-$	3388.41	1632.91	745
$[hmpy]^+$	1681.96	958.67	178				
$[omim]^+$	1838.43	1056.89	183				
$[P_{(14)666}]^+$	4724.97	2641.38	483				

Table 7. Residual and Combinatorial Contributions of Anions for the $[bmim]^+$ Cation at 298 K

anion	μ_{comb}	μ_{res}	abs(μ_{res}) + abs(μ_{comb})	% μ_{res} contribution
$[BF_4]^-$	−3.340	1.345	4.686	28.7
$[TFA]^-$	−3.402	1.157	4.559	25.3
$[L]^-$	−3.430	1.813	5.243	34.5
$[mFAB]^-$	−3.457	0.278	3.735	7.4
$[EtSO_4]^-$	−3.490	1.522	5.013	30.4
$[eFAB]^-$	−3.555	0.101	3.656	2.8
$[Tf_2N]^-$	−3.705	0.251	3.956	6.4
$[OctSO_4]^-$	−3.766	1.215	4.981	24.5
$[mFAP]^-$	−3.791	−0.029	3.821	0.8
$[eFAP]^-$	−4.090	−0.041	4.132	1.0
$[pFAP]^-$	−4.283	−0.085	4.369	2.0
$[bFAP]^-$	−4.443	−0.098	4.541	2.2

where p is the total pressure of CO_2 in gas phase at which the experiment is performed and x is the limiting mole fraction of CO_2 absorbed in the IL. From the above equation, it is clear that the smaller value of H implies the higher solubility of CO_2.

The COSMO volume, surface area, and molecular weight of the anions and cations are given in Table 6. In the present study, we have considered the enthalpy effects arising due to the interaction of CO_2 with the cation/anion and the entropy effects due to size and shape of cation/anion to evaluate the chemical potential. To understand the contribution of enthalpy and entropy effects to the chemical potential, the residual and combinatorial terms (see eq 9) of chemical potentials of various anions for a particular cation $[bmim]^+$ and of various cations for a particular anion $[Tf_2N]^-$ are presented in Tables 7 and 8. It is clear from these tables that the combinatorial term (entropy effect) has much more contribution to chemical potential compared to the residual term (enthalpy effect).

The effect of the alkyl group attached at the R_2 position of the methyl imidazolium cation on the CO_2 solubility has been studied for different anion-containing imidazolium ILs by considering

Table 8. Residual and Combinatorial Contributions of Cations for the $[Tf_2N]^-$ Anion at 298 K

cation	μ_{comb}	μ_{res}	abs(μ_{comb}) + abs(μ_{res})	% μ_{res} contribution
$[emim]^+$	−3.615	0.306	3.922	7.8
$[pmim]^+$	−3.662	0.281	3.943	7.1
$[bmim]^+$	−3.705	0.251	3.956	6.3
$[ETU]^+$	−3.732	0.406	4.138	9.8
$[pemim]^+$	−3.751	0.233	3.984	5.8
$[bmpy]^+$	−3.762	0.223	3.985	5.6
$[pbim]^+$	−3.787	0.212	3.999	5.3
$[hmim]^+$	−3.789	0.212	4.002	5.3
$[ETTU]^+$	−3.793	0.403	4.196	9.6
$[MATMA]^+$	−3.795	0.353	4.148	8.5
$[hmpy]^+$	−3.836	0.211	4.047	5.2
$[VBTMA]^+$	−3.837	0.396	4.233	9.3
$[PTTU]^+$	−3.837	0.370	4.208	8.8
$[omim]^+$	−3.860	0.186	4.046	4.6
$[P_{(14)666}]^+$	−4.365	0.151	4.517	3.3

alkyl groups ranging from ethyl to octyl groups. The computed H values of CO_2 at 298 K and atmospheric pressure for the above cation−anion combinations are presented in Figure 5. For the case of the lactate anion, it can be seen from Figure 5 that, as the alkyl chain length of the group attached to R_2 position increases, Henry's constant continuously decreases and thus the solubility of CO_2 increases. This result is consistent with the experimental H values trend observed for the $[R_n mim]^+[Tf_2N]^- - CO_2$ system.[9,43,34] This is most likely due to the increased CO_2 absorption in the increased free volume created in the IL network by the steric hindrances resulted by longer alkyl chains. Similar trends are also observed for all of the other anions studied.

From Figure 5, a linear eq 17 is fitted for each anion, to find the effect of alkyl chain length at the R_2 position of methyl imidazolium cation (n = 2 to 8).

$$H_n = A + Bn \tag{17}$$

The trend is linear with a coefficient of correlation $R^2 \geq 0.99$, so the extrapolation of the data will give the H values for higher alkyl groups. The slope B and intercept A of eq 17 for different anions are shown in Table 9. Interestingly, from Table 9, it was observed that there is a linear relationship between the slopes and the intercepts of the above 12 anion-based ILs. This observation led us to make a generalized equation for predicting the slope for ILs containing any particular anion and the $[R_n mim]^+$ cation. The linear equation obtained for the slope B with respect to intercept A is given as follows:

$$B = 0.0885 - 0.0493A \tag{18}$$

With the help of eq 18, we can then generalize eq 17 for any anion by combining eqs 18 and 17. Substituting eq 18 in eq 17 and rearranging in such a way that H_n is represented in terms of the H of $[emim]^+$ cation (H_2) and the alkyl chain length n:

$$H_n = (1.1094 - 0.0547n)H_2 + 0.0982(n - 2) \tag{19}$$

where H_2 is the Henry's constant of CO_2 in an IL of an ethyl imidazolium cation and a particular anion. Thus, if we know the H value of [emim] cation-based IL (H_2), then we can predict the value of H_n of higher alkyl chain length imidazolium cation for

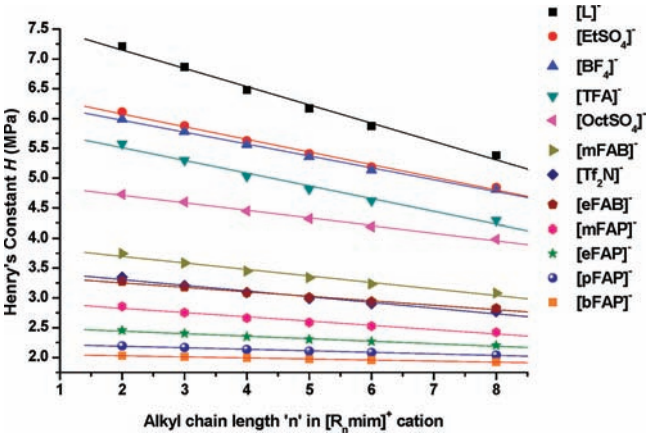

Figure 5. Variation of H values with the chain length of the alkyl group at the R_2 position of the methyl imidazolium cation for different anions of the ILs.

Table 9. Linear Fit Parameters to the H Value Variation for Each Anion with Alkyl Chain Length in Methyl Imidazolium ILs (as in Figure 5)

anion	intercept A	slope B	R^2
$[L]^-$	7.761	−0.307	0.99
$[EtSO_4]^-$	6.503	−0.212	0.99
$[BF_4]^-$	6.365	−0.197	0.99
$[TFA]^-$	5.935	−0.213	0.98
$[OctSO_4]^-$	4.969	−0.126	0.99
$[mFAB]^-$	3.913	−0.108	0.98
$[Tf_2N]^-$	3.500	−0.095	0.98
$[eFAB]^-$	3.403	−0.075	0.99
$[mFAP]^-$	2.971	−0.072	0.97
$[eFAP]^-$	2.523	−0.042	0.98
$[pFAP]^-$	2.240	−0.025	0.99
$[bFAP]^-$	2.059	−0.016	0.98

any anion reasonably well by using above eq 19. The derivation of eq 19 from eqs 17 and 18 is provided in the Supporting Information.

From Table 9, it can be seen that a decrease in slope and intercept is observed when going from nonfluorinated anions to fluorinated anions. This observation is explained as follows. For the nonfluorinated anion, as the alkyl chain length increases, the H value (see Figure 5) decreases more steeply due to the increased free space created by longer alkyl chains. As for the fluorinated anions, the H values are significantly lower than those for the inorganic anions (e.g., BF_4^-). The slope for the variation of H values in fluorinated organic anions with respect to alkyl chain length is less compared to that for nonfluorinated anions. It is well-known that the fluorinated anion-based ILs have high CO_2 solubilities due to the strong interactions of CO_2 with the anion through Lewis acid−base characteristics. The extent of CO_2 solubility obtained due to the fluorination of the anion is usually much higher than that obtained by increasing the alkyl chain length of the cation. This means that the effect of cation becomes insignificant as we go from low fluorination to the high fluorination. Thus, it is not surprising that fluorinated anions show a drastic decrease in slope compared to nonfluorinated anions.

Several studies[5,6,9,43] showed that the solubility of CO_2 is significantly affected by the nature of the anion, while the cation has a small effect. This observation can be seen from the experimental trend of Henry's constants at 298 K shown in Tables 3 and 4. Figure 5 also reveals that, for a particular cationic group, changing anion of the IL has a significant effect on H values of CO_2 (i.e., on the solubility of CO_2); for instance the H value changes from 7.21 to 2.03 by changing the anion of the [emim]-based IL. On the other hand, for a particular anion of the IL, the H values (solubility) of CO_2 are less affected by the alkyl chain length of [mim] cation; for instance, the maximum variation of H value (from 7.21 to 5.38) by changing the alkyl chain length of [mim] cation was observed for the lactate (L^-) anion. It is clear that the effect of the anion is much more pronounced compared to that of the cation on H values (or solubility).

Furthermore, the inorganic/nonfluorinated anions have shown higher Henry's constants (lower CO_2 solubility) compared to those for the organic fluorinated anions. The inorganic/nonfluorinated anions follows a trend as lactate$^-$ > $EtSO_4^-$ > BF_4^- > $OctSO_4^-$. The organic anions follows a trend as TFA^- > Tf_2N^- > $mFAB^-$ > $eFAB^-$ > $mFAP^-$ > $eFAP^-$ > $pFAP^-$ > $bFAP^-$, irrespective of the methyl imidazolium cation studied. It is evident that the presence of fluoroalkyl group in the organic anions affects the H values. The fluorinated molecules have high chemical stability because of the high bond dissociation energy of the C−F bonds. The significantly low molecular interactions due to the mutual repulsive tendency of fluorine atoms lead to higher gas solubilities.[42] As the fluorination of the ion increases, the H value decreases, and thus the solubility increases. This can be explained based on the high electronegativity of the fluorine atom. The CO_2 always tries to position itself to maximize the favorable interactions with the anion; that is, the CO_2 attaches to the highly electronegative fluorine atom of the anion, thus aligning itself to the anion containing fluorine (F) in such a way that the interactions of the positive charge on the carbon atom of CO_2 and the negative charge of the fluorine atom of the anion become higher.[6,42] In fact, many studies (as mentioned in Tables 3 and 4) have shown experimentally that an increase in the fluorination (e.g., fluoroalkyl groups) of the anions of ILs increases the solubility of CO_2.[5,6,9,43] Another important aspect behind the difference in the solubility of CO_2 in various ILs is the molar volume of anions. It is known that that the CO_2 is more soluble in the ILs with solubility parameters (δ) that are close to δ of CO_2. The solubility parameter is inversely proportional to the molar volume ($\delta = (\Delta U^{vap}/v)^{1/2}$). The higher the molar volume of the IL, the lower the solubility parameter and hence more CO_2 solubility.[44]

The predictions of the H value of CO_2 in butyl imidazolium based ILs are shown in Table 10. It can be seen that the inorganic/nonfluorinated anions such as lactate, $EtSO_4^-$, BF_4^-, and $OctSO_4^-$ show higher H values compared to the other fluoroalkyl group-containing organic anions. These observations are similar to those obtained with methyl imidazolium based ILs discussed above. Among all of the anions studied, the bFAP anion has shown the lowest H value, which means the highest solubility. This is because of the fact that bFAP contains highest number (12) of fluoroalkyl groups compared to other anions studied. Consequently, it results in stronger interaction with CO_2 relative to the other ions. From Table 10, it is observed that, for all the anions studied, the Henry's constant of CO_2 in

dx.doi.org/10.1021/je200486c |J. Chem. Eng. Data 2011, 56, 4045–4060

propyl butyl imidazolium (pbim) cation is lower than the propyl methyl imidazolium (pmim) cation containing ILs, suggesting that the alkyl group with a longer chain length exhibits a higher solubility of CO_2. The results presented in Table 10 manifests that the alkyl group chain length of both R_1 and R_2 positions of the imidazolium ring has an influence on the *H* value and thus on the solubility of CO_2.

To understand the effect of amine group tethering to the cation of ILs on the CO_2 solubility, we have predicted Henry's constant of CO_2 in the aminopropyl methyl imidazolium (apmim) and in aminopropyl butyl imidazolium (apbim) (Table 10) cations in combination with different anions. These cations are primary amine-functionalized imidazolium-based ions of the ILs. The comparison of *H* values of CO_2 in (a) pmim with apmim and (b) pbim with apbim for different anions reveals that the amine functionality at the R_2 position of the imidazolium ring produces relatively similar *H* values, though some of the anions show a small decrease in the *H* value. A very few experimental studies available on the application of aminefunctionalized ILs for CO_2 capture showed that the CO_2 solubility increases significantly upon amine-tethering.[7] This increase was, however, mainly due to the formation of the ammonium carbamate and the other ammonium-anchored species, confirmed by Fourier transform infrared (FT-IR) and ^{13}C NMR spectroscopy studies.[7] Thus, for amine-tethered ILs the *H* value alone cannot explain the solubility differences observed experimentally due to the participation of chemically formed carbamate type species in capturing CO_2.

In addition, the effect of the functional group present at the R_2 position of butyl imidazolium on the *H* value is studied, and the data are presented in Table 10. For the three functional groups (aminopropyl, dimethylaminopropyl, and vinyl benzyl) considered, the *H* value of CO_2 is in the order: vinyl benzyl < dimethylaminopropyl (tertiary amine) < aminopropyl (primary amine). These results suggest that the IL interaction with CO_2 (solubility) can be enhanced by functionalizing the ILs with a proper choice of functional group. In this case, vinyl benzene- and then tertiary amine-tethered ILs showed superior performance for CO_2 capture than their corresponding non-functionalized ILs. Vinyl benzyl functionalized imidazolium ILs are being used in synthesizing poly(ionic liquids). Similar trends are observed for all the anions studied. Both the methyl- and the butyl-imidazolium-based cations series with different anion combinations revealed that pFAP and bFAP anions containing ILs have shown the lowest *H* values (highest CO_2 solubilities).

The *H* values of CO_2 in uronium-, thiouronium-, pyridinium-, ammonium-, and phosphonium-based ILs are shown in Table 11. It is apparent that both uronium (ETU) and thiouronium (ETTU) cations show similar *H* values. It suggests that the heteroatom of the uronium-based cation has a minor effect on the *H* value. Specifically, the uronium- and thiouronium-based cations of ILs with $EtSO_4$ and BF_4 anion combination show a different trend in *H* values when compared with those of imidazolium-based ILs. This result suggests that the combined effect of the uronium and thiouronium-based cations and $EtSO_4$ and BF_4 anion interactions with the CO_2 molecule is different from the interactions resulted from other cations with these anion combinations. Furthermore, a comparison of the *H* values of ETTU and PTTU in Table 11 shows that the alkyl group of the thiouronium cation has shown a small effect on the *H* value. Uronium- and thiouronium-series ILs also showed that the pFAP and bFAP anion-containing ILs exhibit the lowest *H* values (i.e., the highest solubilities).

Three more series of pyridinium, ammonium, and phosphonium cation-based ILs are also studied, and the computed *H* values are also given in Table 11. For all three pyridinium, ammonium, and phosphonium cations, the trend in *H* values with respect to the anion present in the IL follow the same trend as that of imidazolium-based cations. As the eq 19 is applicable for any anion but only for $[R_n mim]^+$ cation-based ILs, we have

Table 10. Predicted Henry's Constant (in MPa) of CO_2 in Butyl Imidazolium ILs Having Different Functional Groups at 298 K and 1 atm

ion	$[pmim]^+$	$[pbim]^+$	$[apmim]^+$	$[apbim]^+$	$[dmapbim]^+$	$[vbbim]^+$
$[L]^-$	6.86	5.96	6.55	5.78	5.54	4.63
$[EtSO_4]^-$	5.88	5.22	5.35	4.84	4.68	4.28
$[BF_4]^-$	5.78	5.12	5.13	4.66	4.49	4.28
$[TFA]^-$	5.30	4.65	5.24	4.63	4.40	3.95
$[OctSO_4]^-$	4.60	4.22	4.37	4.04	3.94	3.64
$[mFAB]^-$	3.58	3.22	3.54	3.20	3.04	3.01
$[Tf_2N]^-$	3.21	2.94	3.22	2.94	2.82	2.76
$[eFAB]^-$	3.18	2.90	3.16	2.93	2.77	2.74
$[mFAP]^-$	2.75	2.53	2.83	2.60	2.47	2.42
$[eFAP]^-$	2.40	2.28	2.48	2.35	2.26	2.21
$[pFAP]^-$	2.17	2.10	2.23	2.16	2.10	2.04
$[bFAP]^-$	2.01	1.97	2.07	2.02	1.99	1.93

Table 11. Predicted Henry's Constant (in MPa) of CO_2 in Various Cation Groups of ILs at 298 K and 1 atm

ion	$[ETU]^+$	$[ETTU]^+$	$[PTTU]^+$	$[bmpy]^+$	$[hmpy]^+$	$[VBTMA]^+$	$[MATMA]^+$	$[P_{(14)666}]^+$
$[L]^-$	6.55	6.37	6.11	6.23	5.76	5.87	5.54	3.46
$[EtSO_4]^-$	4.84	4.72	4.57	5.20	4.95	5.33	4.99	3.20
$[BF_4]^-$	4.63	4.53	4.39	5.02	4.81	5.41	5.00	3.09
$[TFA]^-$	5.35	5.17	4.95	4.85	4.54	4.91	4.74	3.03
$[OctSO_4]^-$	4.16	4.06	3.95	4.24	4.07	4.25	4.09	2.93
$[mFAB]^-$	3.57	3.47	3.34	3.28	3.14	3.56	3.50	2.38
$[Tf_2N]^-$	3.25	3.17	3.07	2.98	2.88	3.10	3.10	2.27
$[eFAB]^-$	3.34	3.23	3.11	2.98	2.85	3.17	3.16	2.20
$[mFAP]^-$	2.99	2.90	2.80	2.62	2.51	2.75	2.75	2.04
$[eFAP]^-$	2.64	2.58	2.52	2.34	2.27	2.40	2.41	1.96
$[pFAP]^-$	2.39	2.34	2.30	2.14	2.10	2.17	2.18	1.88
$[bFAP]^-$	2.21	2.18	2.15	2.00	1.97	2.01	2.02	1.82

dx.doi.org/10.1021/je200486c |*J. Chem. Eng. Data* 2011, 56, 4045–4060

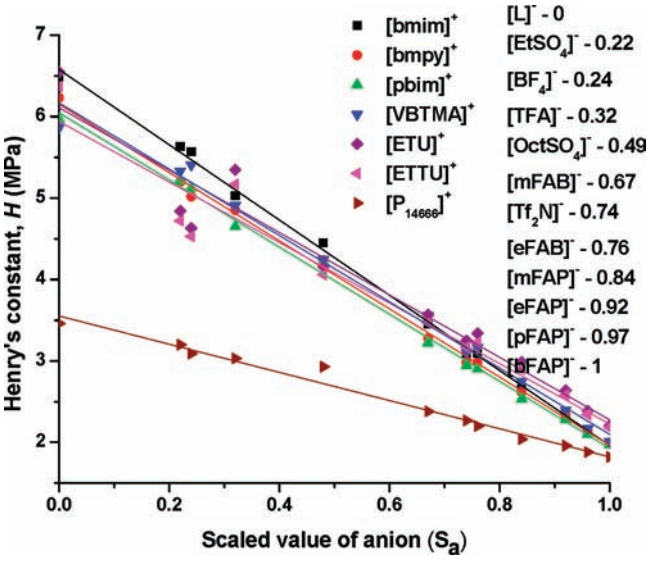

Figure 6. *H* values of various cations with scaled inorganic and organic anions of ILs. Scaled values of anion are shown in the plot.

developed an approach to predict the *H* value for any type of cation and anion. The approach is given as follows.:

By using the intercept values obtained for $[R_n mim]^+$ cation-based ILs (from Figure 5 and Table 9), all of the anions are scaled between 0 and 1 by fixing the lactate anion at 0 (corresponding to the highest *H* value in the series, $A_{[L]^-}$) and the bFAP anion at 1 (corresponding to the lowest *H* value in the series, $A_{[bFAP]^-}$). The scaled value of any anion (S_a) is defined as:

$$\text{scaled value of anion, } S_a = \frac{A_{[L]^-} - A_{anion}}{A_{[L]^-} - A_{[bFAP]^-}} \quad (20)$$

where A_{anion} is the intercept value for the anion of interest with combination of any $[R_n mim]^+$ cation. It can be obtained from eq 19 using the H_2 value and $n = 0$ (since H_n at $n = 0$ is nothing but the intercept value). The scaled values of all of the anions (ranging from 0 to 1) are shown in the legend of Figure 6. Furthermore, the *H* values of different cations such as $[bmim]^+$, $[bmpy]^+$, $[pbim]^+$, $[ETU]^+$, $[ETTU]^+$, $[VBTMA]^+$, and $[P_{(14)666}]^+$ against scaled anions (all 12 anions studied) are presented in Figure 6. From Figure 6, we can observe that, with the scaled anions, all of the cations are following a straight line trend. The linear fit parameters $A_{[ca]^+}$ and $B_{[ca]^+}$ of various cations according to the following equation are given in Table 12.

$$H_{[ca]^+[a]^-} = A_{[ca]^+} + B_{[ca]^+} \times S_a \quad (21)$$

By using eq 21, Henry's constant of CO_2 with any cation and any anion combination $H_{[ca]^+[a]^-}$ can be calculated. In brief, initially the scaled value S_a of that particular anion is obtained on 0 to 1 scale by using eq 20. In the next step, $H_{[ca]^+[a]^-}$ can be calculated by using the $A_{[ca]^+}$ and $B_{[ca]^+}$ of the particular cation, which can be obtained from Table 12 and the S_a of the particular anion. This indeed significantly reduces the computational effort in obtaining Henry's constants for the new IL systems. From Figure 6, it can be seen that the phosphonium cation is the most preferable one since it has lowest *H* values. Furthermore, among the different series of IL systems studied, the *H* values of CO_2 for the best cation of each series of ILs with $OctSO_4$ (best anion in nonfluorinated systems) and bFAP (best anion in fluorinated systems) anion combinations

Table 12. Linear Parameters for Various Cations with Scaled Anions

cation	intercept $A_{[ca]^+}$	slope $B_{[ca]^+}$	R^2
$[emim]^+$	7.23	−5.20	0.99
$[pmim]^+$	6.91	−4.91	0.99
$[bmim]^+$	6.57	−4.62	0.99
$[pemim]^+$	6.29	−4.33	0.99
$[hmim]^+$	6.00	−4.05	0.99
$[omim]^+$	5.55	−3.63	0.99
$[apmim]^+$	6.42	−4.31	0.99
$[pbim]^+$	6.04	−4.11	0.99
$[apbim]^+$	5.71	−3.68	0.99
$[dmapbim]^+$	5.48	−3.52	0.99
$[vbbim]^+$	4.85	−2.84	0.99
$[bmpy]^+$	6.15	−4.18	0.99
$[hmpy]^+$	5.77	−3.82	0.99
$[MATMA]^+$	5.78	−3.62	0.99
$[VBTMA]^+$	6.16	−4.07	0.99
$[ETU]^+$	6.10	−3.83	0.95
$[ETTU]^+$	5.94	−3.71	0.95
$[PTTU]^+$	5.71	−3.53	0.95
$[P_{(14)666}]^+$	3.55	−1.73	0.98

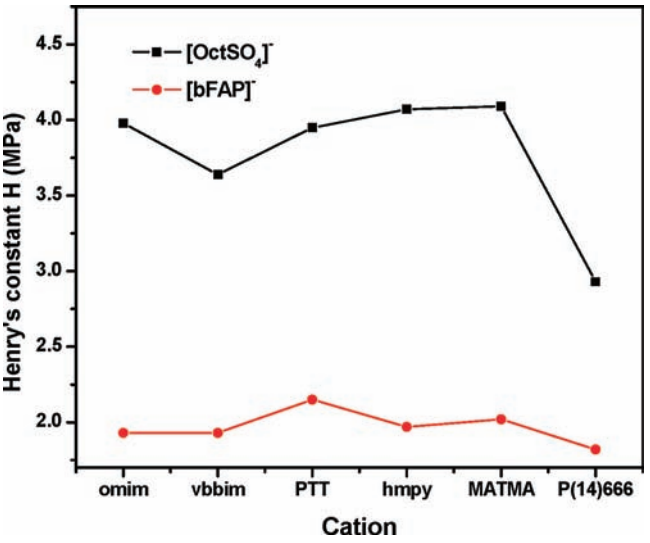

Figure 7. Effect of the nature of cation and anion of the IL on the Henry's constant of CO_2.

are presented in Figure 7. It is clearly demonstrated in Figure 7 that the *H* value strongly depends on the nature of the anion, with organic anion containing fluoro alkyl groups (bFAP) being the most preferable one for the highest CO_2 solubility. For the cation effect, although the nature of the cation has less effect on the *H* value for most of the cations compared to the anions of ILs, the phosphonium-based ($[P_{(14)666}]^+$) cation has a strong influence on the *H* value (lowest). Due to high entropic effects arising due to its high surface area and volume, the $P_{(14)666}$ cation is a promising cation for achieving good CO_2 solubility compared to the other cations. Thus, of all the ions studied, the $P_{(14)666}$ cation and pFAP and bFAP anions have shown the highest CO_2 solubilities as they exhibit the lowest *H* values.

dx.doi.org/10.1021/je200486c |J. Chem. Eng. Data 2011, 56, 4045–4060

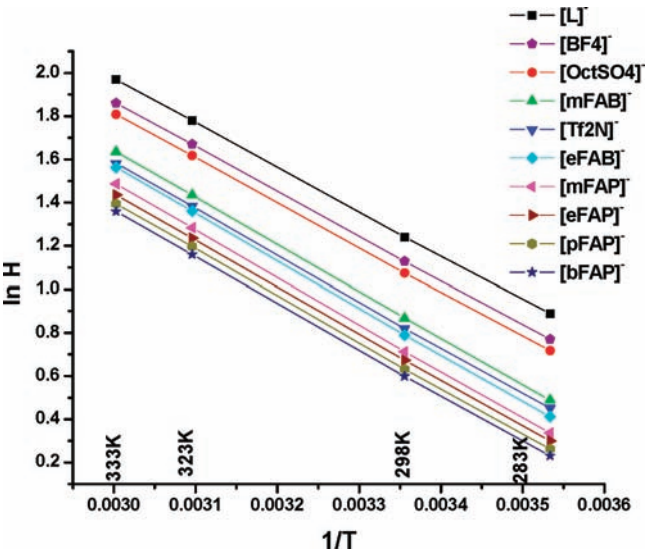

Figure 8. Effect of temperature on Henry's constant for phosphonium ILs.

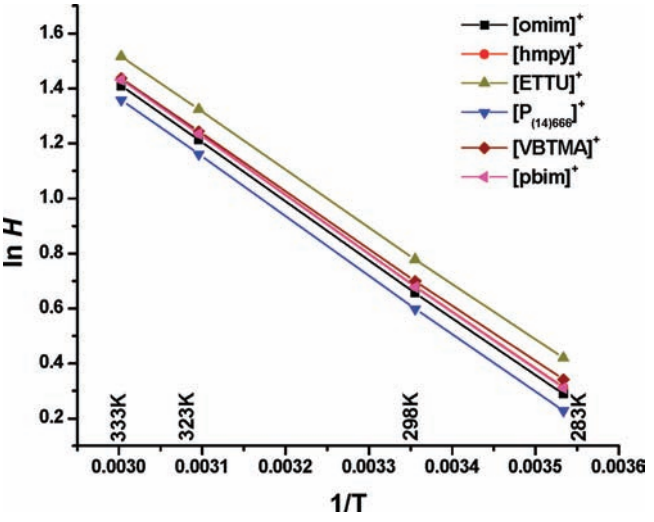

Figure 9. Effect of temperature on Henry's constant for bFAP anion-based ILs.

Henry's constant values of CO_2 in various ILs are studied at four different temperatures, (283, 298, 323, and 333) K, respectively. The lowest H values are obtained at 283 K. The H values increase with the increase of temperature ($H_{283} < H_{298} < H_{323} < H_{333}$). From these results it is clear that the low temperatures favor high solubility, which was also reported in the literature;[6,36,37] As the temperature increases, the IL will not expand (ILs are stable at these temperatures), but the kinetic energy of the gas molecules would increase, resulting in a more rapid motion of the gas molecules, breaking the intermolecular bonds/attraction which enable gas molecules to escape from the solvent/liquid. Indeed this is a typical behavior for the absorption of most of the gases in liquid systems, though it depends on the nature of solvent and gas. The measured H values for the phosphonium cation $P_{(14)666}$ with different anions are plotted as a function of temperature in a range of (283 to 343) K as ln H versus $1/T$ plot which is shown in Figure 8. A linear equation is fitted according to eq 22 with a coefficient of correlation $R^2 > 0.99$. Similarly the effect of temperature on the H value for the bFAP anion with different cations is plotted as ln H versus $1/T$ graph in Figure 9. A linear equation is fitted according to eq 22 in a range of (283 to 343) K for each cation with a coefficient of correlation of $R^2 > 0.99$. The fitting parameters for the phosphonium cation and bFAP anion are shown in Table 13.

$$\ln H = A + B(1/T) \tag{22}$$

The physical significance of eq 22 can be explained from the following equation:

$$H = p^{sat} \exp\left(\frac{\mu_S^X - \mu_X^X}{RT}\right) \tag{23}$$

Table 13. Linear Fit Parameters for the Effect of Temperature on H of the ILs

$[P_{(14)666}]^+$ cation				[bFAP]$^-$ anion			
	intercept				intercept		
anion	A	slope B	R^2	cation	A	slope B	R^2
$[L]^-$	8.1	−2043	0.99	$[VBTMA]^+$	7.64	−2067.4	0.99
$[OctSO_4]^-$	8	−2060.6	0.99	$[ETTU]^+$	7.74	−2072.1	0.99
$[mFAB]^-$	8.14	−2165.3	0.99	$[hmpy]^+$	7.78	−2115.3	0.99
$[Tf_2N]^-$	8	−2136.6	0.99	$[pbim]^+$	7.79	−2117.6	0.99
$[eFAB]^-$	8.09	−2173.8	0.99	$[omim]^+$	7.77	−2118	0.99
$[mFAP]^-$	8.01	−2171.5	0.99	$[P_{(14)666}]^+$	7.77	−2135.5	0.99
$[eFAP]^-$	7.87	−2143.3	0.99				
$[pFAP]^-$	7.82	−2140.1	0.99				
$bFAP]^-$	7.75	−2130.3	0.99				
$[BF_4]^-$	8.04	−2058.4	0.99				

Table 14. Average Slope (B) of Various Cations and Anions

sample no.	cation	average slope for all anions
1	$[emim]^+$	−2102.01
2	$[pmim]^+$	−2106.70
3	$[bmim]^+$	−2107.32
4	$[pemim]^+$	−2106.97
5	$[hmim]^+$	−2099.73
6	$[omim]^+$	−2103.74
7	$[pbim]^+$	−2119.32
8	$[ETU]^+$	−2097.85
9	$[ETTU]^+$	−2092.97
10	$[PTTU]^+$	−2098.19
11	$[bmpy]^+$	−2123.05
12	$[hmpy]^+$	−2119.36
13	$[VBTMA]^+$	−2049.34
14	$[MATMA]^+$	−2081.07
15	$[P_{(14)666}]^+$	−2114.58
16	$[L]^-$	−2054.00
17	$[mFAB]^-$	−2154.91
18	$[bFAP]^-$	−2104.84
	tot average (B_{avg})	−2102.00

dx.doi.org/10.1021/je200486c |J. Chem. Eng. Data 2011, 56, 4045–4060

Table 15. Temperature-Dependent H Values from COSMO-RS against the Proposed Universal Equation 24[a]

T		[omim]$^+$[L]$^-$			[hmpy]$^+$[mFAB]$^-$			[$P_{(14)666}$]$^+$[bFAP]$^-$		
K	$\exp(B_{avg}(1/T - 1/T_r)$	$H_{universal}$	H_{COSMO}	% err	$H_{universal}$	H_{COSMO}	% err	$H_{universal}$	H_{COSMO}	% err
283	0.6881	3.70	3.74	0.92	2.16	2.13	1.52	1.25	1.25	0.24
298	1.0000	5.38	5.38	0.06	3.13	3.13	0.17	1.82	1.82	0.26
323	1.7262	9.29	9.15	1.51	5.42	5.52	1.78	3.14	3.17	0.99
333	2.0988	11.29	11.07	2.03	6.59	6.76	2.47	3.82	3.87	1.25
348	2.7551	14.82	14.42	2.76	8.65	8.96	3.42	5.01	5.10	1.61

[a] $H_{universal}$: from eq 24; HCOSMO: prediction from COSMO-RS; B_{avg}: universal slope = −2102.

Equation 23 can be rewritten by taking the natural logarithm (ln) on both sides;

$$\ln H = \ln p^{sat} + \left(\frac{\mu_S^X - \mu_X^X}{R}\right)\frac{1}{T} \quad (24)$$

In eq 22 the intercept A refers to the Henry's constant H at infinite temperature, and the slope B refers to the chemical potential of CO_2 in the IL. Since infinite temperature is not a feasible temperature, we can ignore the intercept A by bringing the concept of reference temperature. From eqs 23 and 24, we can observe that μ_X^X is a constant at a particular temperature and is independent of the IL studied. Hence we can say that the H value only depends on the chemical potential of CO_2 in the particular IL, that is, μ_S^X. Thus the slope B in eq 22 is affected by μ_S^X of CO_2 in that particular IL.

The slopes of ln H versus $1/T$ for a particular cation with each anion and vice versa were obtained. By taking the average of all of the slopes as B_{avg} and 298 K as the reference temperature T_r, an expression for H is proposed as:

$$H = H_r \exp\left(B_{avg}\left(\frac{1}{T} - \frac{1}{T_r}\right)\right) \quad (25)$$

where H_r is the Henry's constant of particular cation and anion at the reference temperature T_r(298 K). B_{avg} is a universal average slope which is obtained by taking the average slope of all of the cations and anions. The B value of all of the 15 cations and 3 anions are given in Table 14. Equation 25 indicates that, for a particular cation, all of the anions behave in the same way with respect to temperature and for a particular anion, all of the cations behave in the same way with respect to temperature. By using eq 25 we can predict the H value of CO_2 in any IL at any temperature by just knowing its H value at the reference temperature 298 K. The percent deviation of the H values obtained from eqs 22 and 25 is observed to be between (0.01 and 3.5) %. A comparison table is given in Table 15.

6. CONCLUSIONS

In the present study, the Henry's constant values of CO_2 at four different temperatures [(283, 298, 323, and 333) K] and at 1 atm in 228 ILs have been successfully determined with our own developed code using COSMO-RS theory. The good agreement of the computed Henry's constants with the reported experimental data suggests that the results obtained for the H values are reliable and can be used as good indicators for the CO_2 solubility when designing new ILs. The rmsd of the results from the experimental literature data came out as 0.35 and an MUPE of less than 10 %. The present study demonstrated that the H value of CO_2 in ILs is strongly dependent on the nature of anion. The organic anions having fluoroalkyl groups results in lower H values (higher CO_2 solubility) than the nonfluorinated/inorganic anions. On the other hand, the nature of cation has a less effect on the H value compared to the anions of ILs. Among the cations studied, the phosphonium-based cation has a strong influence on the H value (lowest) relative to the other cations due to the increased entropic effects arising from its large surface area and volume. Among the ILs studied, the phosphonium-based ([$P_{(14)666}$]$^+$) cation and pFAP and bFAP anion-based ILs have shown the lowest H values, suggesting that these ions have strong interactions with CO_2, which result in the highest solubility of CO_2. Comparing the H values at different temperatures, it is clear that the low temperatures favor high solubility. A predictive equation has successfully been developed to determine the H of [$R_n$mim]$^+$ cation-based ILs by using the H value of CO_2 in the [R_2mim]$^+$ IL system. The effect of amine functionalization on imidazolium cation has been studied. It was observed that the tertiary amine tethered ILs show high CO_2 solubility (low H values) compared to untethered and primary amine tethered ILs. A single parameter based correlation has been developed to predict the H values at various temperatures by just knowing the H value at the reference temperature 298 K. The percent errors by using these equations are found to be between (0.01 and 3.5) %.

■ ASSOCIATED CONTENT

Supporting Information. (a) The optimization procedure for the two parameters λ_1 and λ_2. (b) A comparison of the H values obtained with cosmo files generated by using aug-cc-pVTZ and TZVP basis sets. (c) A detailed derivation of eq 19 from eqs 17 and 18. (d) Henry's constant values of CO_2 in the 228 ILs studied at temperatures of (283, 323, and 333) K. A comparison between the H value predictions obtained based on two basis sets are given. This material is available free of charge via the Internet at http://pubs.acs.org.

■ AUTHOR INFORMATION

Corresponding Author
*E-mail: akhanna@iitk.ac.in.

■ REFERENCES

(1) Litynski, J. T.; Plasynski, S.; Howard, G. M.; Mahoney, C.; Srivastava, R. D. The United States Department of Energy's Regional Carbon Sequestration Partnerships Program Validation Phase. *Environ. Int.* **2008**, *34*, 127–138.

(2) Pennline, H. W.; Luebke, D. R.; Morsi, B. I.; Heinntz, Y. J.; Jones, K. L.; Ilconich, J. B. *Carbon dioxide capture and separation techniques for*

advanced power generation point sources; Technical report; United States Department of Energy, NETL: Washington, DC, 2006.

(3) Pennline, H. W.; Luebke, D. R.; Morsi, B. I.; Heinntz, Y. J.; Jones, K. L.; Ilconich, J. B. *Carbon dioxide capture and separation techniques for gasification based power generation point sources*; Technical report; United States Department of Energy, NETL: Washington, DC, 2007.

(4) Maginn, E. J. *Design and evaluation of ionic liquids as novel CO_2 absorbents*; Quarterly Technical Report; University of Notre Dame: Notre Dame, IN, December 31, 2004.

(5) Anderson, J. L.; Dixon, J. K.; Maginn, E. J.; Brennecke, J. F. Measurement of SO_2 solubility in ionic liquids. *J. Phys. Chem. B* **2006**, *110*, 15059–15062.

(6) Cadena, C.; Anthony, J. L.; Jindal, K. S.; Timothy, I. M.; Brennecke, J. F.; Maginn, E. J. Why is CO_2 So Soluble in Imidazolium-Based Ionic Liquids? *J. Am. Chem. Soc.* **2004** *126*, 5300–5308.

(7) Bates, E. D.; Mayton, R. D.; Ioanna, N.; Davis, J. H. CO_2 Capture by a Task-Specific Ionic Liquid. *J. Am. Chem. Soc.* **2002**, *124*, 926–927.

(8) Bhargava, B. L.; Balasubramanian, S. Probing anion−carbon dioxide interactions in room temperature ionic liquids: Gas phase cluster calculations. *Chem. Phys. Lett.* **2007**, *444*, 242–246.

(9) Muldoon, M. J.; Sudhir, N. V. K.; Anderson, J. L.; Dixon, J. K.; Brennecke, J. F. Improving Carbon Dioxide Solubility in Ionic Liquids. *J. Phys. Chem. B* **2007**, *111*, 9001–9009.

(10) Mortan, S. A. *Evaluation of ionic liquids for green separations*; Dept. of Chemical Engineering, Lafayette College, Centre for applied energy research: Easton, PA, 2008.

(11) Sona, R.; Schilderman, A.; Peters, C. J. A potential ionic liquid for CO_2-separating membranes: selection and gas solubility studies, Physical Chemistry & Molecular Thermodynamics. Delft University of Technology. *GCEP Res. Symp.*, Sept **2006**; http://gcep.stanford.edu/pdfs/N-9p6x1EoFMn6wKtz4_wwQ/2.8-Raeissi_Peters-web-version.pdf.

(12) Klamt, A. Conductor-like Screening Model for Real Solvents: A New Approach to the Quantitative Calculation of Solvation Phenomena. *J. Phys. Chem.* **1995**, *99*, 2224–2235.

(13) Zhang, X.; Liu, Z.; Wang, W. Screening of Ionic Liquids to Capture CO_2 by COSMO-RS and Experiments. *AIChE J.* **2008**, *54*, 2717–2728.

(14) Palomar, J.; Miquel, M. G.; Polo, A.; Rodriguez, F. Understanding the physical absorption of CO_2 in ionic liquids using the COSMO-RS method. *Ind. Eng. Chem. Res.* **2011**, *50*, 3452–3463.

(15) Manan, N. A.; Hardacre, C.; Jacquemin, J.; Rooney, D. W.; Youngs, T. G. A. Evaluation of Gas Solubility Prediction in Ionic Liquids using COSMOthermX. *J. Chem. Eng. Data* **2009**, *54*, 2005–2022.

(16) Ayman, G. Evaluating COSMO-RS for vapor liquid equilibrium and TURBOMOLE for ideal gas properties. Masters Thesis, University of Akron, Akron, OH, 2007.

(17) Klamt, A.; Eckert, F. COSMO-RS: a novel and efficient method for the a priori prediction of thermophysical data of liquids. *Fluid Phase Equilib.* **2000**, *172*, 43–72.

(18) Eckert, F.; Klamt, A. Fast Solvent Screening via Quantum Chemistry: COSMO-RS Approach. *AIChE J.* **2002**, *48*, 369–385.

(19) Schafer, A.; Klamt, A.; Sattel, D.; Lohrenz, J. C W.; Eckert, F. COSMO Implementation in TURBOMOLE: Extension of an efficient quantum chemical code towards liquid systems. *Phys. Chem. Chem. Phys.* **2000**, *2*, 2187–2193.

(20) Klamt, A.; Eckert, F. Prediction of vapor liquid equilibria using COSMOtherm. *Fluid Phase Equilib.* **2004**, *217*, 53–57.

(21) Dana, C.; Klamt, A.; Geana, D. Vapor−liquid equilibrium prediction at high pressures using activity coefficients at infinite dilution from COSMO-type methods. *Fluid Phase Equilib.* **2005**, *231*, 231–238.

(22) Freirea, M. G.; Venturaa, S. P. M.; Luis, M. N. B. F.; Marruchoa, I. M.; Coutinhoa, J. A. P. Evaluation of COSMO-RS for the prediction of LLE and VLE of water and ionic liquids binary systems. *Fluid Phase Equilib.* **2008**, *268*, 74–84.

(23) Mehler, C.; Klamt, A.; Peukert, W. Use of COSMO-RS for the Prediction of Adsorption Equilibria. *AIChE J.* **2002**, *48*, 1093–1099.

(24) Klamt, A.; Eckert, F.; Arlt, W. COSMO-RS: An Alternative to Simulation for Calculating Thermodynamic Properties of Liquid Mixtures. *Annu. Rev. Chem. Biomol. Eng.* **2010**, *1*, 101.

(25) Klamt, A.; Jonas, V.; Burger, T.; Lohrenz, J. H. Refinement and parameterization of COSMO-RS. *J. Phys. Chem. A* **1998**, *102*, 5074–5085.

(26) Eckert, F. *COSMOtherm users manual*, Version C2.1, release 01.10; COSMO logic GmbH: Darmstadt, Germany, 2009.

(27) Diedenhofen, M.; Eckert, F.; Klamt, A. Prediction of infinite dilution activity coefficients of organic compounds in ionic liquids using COSMO-RS. *J. Chem. Eng. Data* **2003**, *48*, 475–479.

(28) Banerjee, T.; Verma, K. K.; Khanna, A. Liquid−Liquid Equilibrium for Ionic Liquid Systems Using COSMO-RS: Effect of Cation and Anion Dissociation. *AIChE J.* **2008**, *54*, 1874–1885.

(29) Banerjee, T.; Sahoo, R. K.; Rath, S. S.; Rakesh, K.; Khanna, A. Multicomponent Liquid-Liquid Equilibria Prediction for Aromatic Extraction Systems Using COSMO-RS. *Ind. Eng. Chem. Res.* **2007**, *46*, 1292–1304.

(30) Frisch, M. J.; Trucks, G. W.; Schlegel, H. B.; Scuseria, G. E.; Robb, M. A.; Cheeseman, J. R.; Montgomery, J. A.; Vreven, T.; Kudin, K. N.; Burant, J. C.; Millam, J. M.; Iyengar, S. S.; Tomasi, J.; Barone, V.; Mennucci, B.; Cossi, M.; Scalmani, G.; Rega, N.; Petersson, G. A.; Nakatsuji, H.; Hada, M.; Ehara, M.; Toyota, K.; Fukuda, R.; Hasegawa, J.; Ishida, M.; Nakajima, T.; Honda, Y.; Kitao, O.; Nakai, H.; Klene, M.; Li, X.; Knox, J. E.; Hratchian, H. P.; Cross, J. B.; Adamo, C.; Jaramillo, J.; Gomperts, R.; Stratmann, R. E.; Yazyev, O.; Austin, A. J.; Cammi, R.; Pomelli, C.; Ochterski, J. W.; Ayala, P. Y.; Morokuma, K.; Voth, G. A.; Salvador, P.; Dannenberg, J. J.; Zakrzewski, V. G.; Dapprich, S.; Daniels, A. D.; Strain, M. C.; Farkas, O.; Malick, D. K.; Rabuck, A. D.; Raghavachari, K.; Foresman, J. B.; Ortiz, J. V.; Cui, Q.; Baboul, A. G.; Clifford, S.; Cioslowski, J.; Stefanov, B. B.; Liu, G.; Liashenko, A.; Piskorz, P.; Komaromi, I.; Martin, R. L.; Fox, D. J.; Keith, T.; Al-Laham, M. A.; Peng, C. Y.; Nanayakkara, A.; Challacombe, M.; Gill, P. M. W.; Johnson, B.; Chen, W.; Wong, M. W.; Gonzalez, C.; Pople, J. A. *Gaussian 03*, Revision C.02; Gaussian Inc: Wallingford, CT, 2004.

(31) Schaftenaar, G.; Noordik, J. H. Molden: a pre- and post-processing program for molecular and electronic structures. *J. Comput.-Aided Mol. Des.* **2000**, *14*, 123–134.

(32) Becke, A. D. Density-functional thermo chemistry.III. the role of exact exchange. *J. Chem. Phys.* **1993**, *98*, 5648–5652.

(33) Lee, C.; Yang, W.; Parr, R. G. Development of the Colle-Salvetti correlation- energy formula into a functional of the electron density. *Phys. Rev. B* **1988**, *37*, 785–789.

(34) Hariharan, P. C.; Pople, J. A. Accuracy of AH, equilibrium geometries by single determinant molecular orbital theory. *Mol. Phys.* **1974**, *27*, 209.

(35) Perdew, J. P. Density-functional approximation for the correlation energy of the inhomogeneous electron gas. *Phys. Rev. B* **1986**, *33*, 8822–8824.

(36) Schaefer, A.; Horn, H.; Ahlrichs, R. Fully optimized contracted Gaussian basis sets for atoms Li to Kr. *J. Chem. Phys.* **1992**, *97*, 2571–2577.

(37) Godbout, N.; Salahub, D. R.; Andzelm, J.; Wimmer, E. Optimization of Gaussian type basis sets for local spin density functional calculations. Part 1. Boron through Neon optimization technique and validation. *Can. J. Chem.* **1992**, *70*, 560–571.

(38) Carvalho, P. J.; Coutinho, J. A. P. On the nonideality of CO_2 solutions in ionic liquids and other low volatile solvents. *J. Phys. Chem. Lett.* **2010**, *1*, 774–780.

(39) Millera, M. B.; Chena, D. L.; Xiea, H. B.; Luebkea, D. R.; Johnsona, J. K.; Enick, R. M. Solubility of CO_2 in CO_2-philic oligomers; COSMOtherm predictions and experimental results. *Fluid Phase Equilib.* **2009**, *287*, 26–32.

(40) Baltus, R. *Room temperature ionic liquids*, a report; http://people.clarkson.edu/∼rbaltus/Room%20Temperature%20Ionic%20Liquids.pdf.

(41) Gomes, M. F. C. Low-pressure solubility and thermodynamics of salvation of carbon dioxide, ethane and hydrogen in 1-hexyl-3methyl imidazolium Bis (trifluoro methyl sulfonyl) amide between temperatures of 283 K and 343 K. *J. Chem. Eng. Data* **2007**, *52*, 472–475.

(42) Almantariotis, D.; Gefflaut, T.; Padua, A. A. H.; Coxam, J. Y.; Costa Gomes, M. F. Effect of fluorination and size of the alkyl side-chain

on the solubility of carbon dioxide in 1-alkyl, 3-methyl imidazolium bis(trifluoromethylsulfonyl) imide ionic liquids. *J. Phys. Chem. B* **2010**, *114*, 3608–3617.

(43) Baltus, R. E.; Benjamin, H. C.; Sheng, D.; Luo, H.; DePaoli, D. W. Low-Pressure Solubility of Carbon Dioxide in Room-Temperature Ionic Liquids Measured with a Quartz Crystal Microbalance. *J. Phys. Chem. B* **2004**, *108*, 721–727.

(44) Anthony, J. L.; Anderson, J. L.; Maginn, E. J.; Brennecke, J. F. Anion effects on gas solubility in ionic liquids. *J. Phys. Chem. B* **2005**, *109*, 6366–6374.

(45) Anderson, J. L.; Dixon, J. K.; Brennecke, J. F. Solubility of CO_2, CH_4, C_2H_6, C_2H_4, O_2, and N_2 in 1-Hexyl-3-methylpyridinium Bis-(trifluoromethylsulfonyl)imide: Comparison to Other Ionic Liquids. *Acc. Chem. Res.* **2007**, *40*, 1208–1216.